ISSUE: January 2018

# Estimating Output Current Tolerance Of A Primary–Side-Regulated Constant-Current Flyback Converter (Part 1): The Analytical Model

*by Stéphanie Cannenterre, ON Semiconductor, Toulouse, France*

The primary-side-regulated (PSR) flyback converter is a popular converter widely used in the LED drive market and in the portable electronic market for travel adapters. Primary-side regulation consists of regulating the output current or the output voltage of the flyback by observing waveforms from the primary side of the converter. Thus, this technique helps decrease the bill of materials of the power supply by removing the optocoupler, the TL431 or the operational amplifier sensing the output voltage. Besides, it also saves the resistor needed to sense the output current.

It is well known that an image of the output voltage can be obtained through the observation of the auxiliary winding. The output current can be estimated by sensing the current in the primary-side MOSFET. However, what precision on the controlled parameter can be expected with this technique?

LED driver manufacturers are usually targeting ±5% at a given input voltage. Using worst-case circuit analysis techniques, this paper will detail how to estimate the accuracy of the flyback output current and compare the obtained results against the ±5% target. The first part of this article will introduce an analytical model of the primary-side constant-current flyback control scheme. Subsequent parts of this article will present a Monte Carlo Analysis of the converter output current followed by an extreme value analysis and a sensitivity analysis.

## PSR Flyback

Reference [1] describes the differences between secondary-side regulation and a primary-side version of the flyback converter. Fig. 1 shows the schematic of a flyback converter implementing secondary-side constant-current (CC) and constant-voltage (CV) regulation. The secondary-side bill of materials is quite important: one operational transconductance amplifier (OTA) (with its associated compensation network) senses the output voltage while the other one senses the output current. The OTA sinking the most current wins over the other one and imposes its regulation setpoint through the optocoupler. A resistor is needed for output current sensing; depending on the output current value, its power dissipation can decrease the efficiency of the power supply.

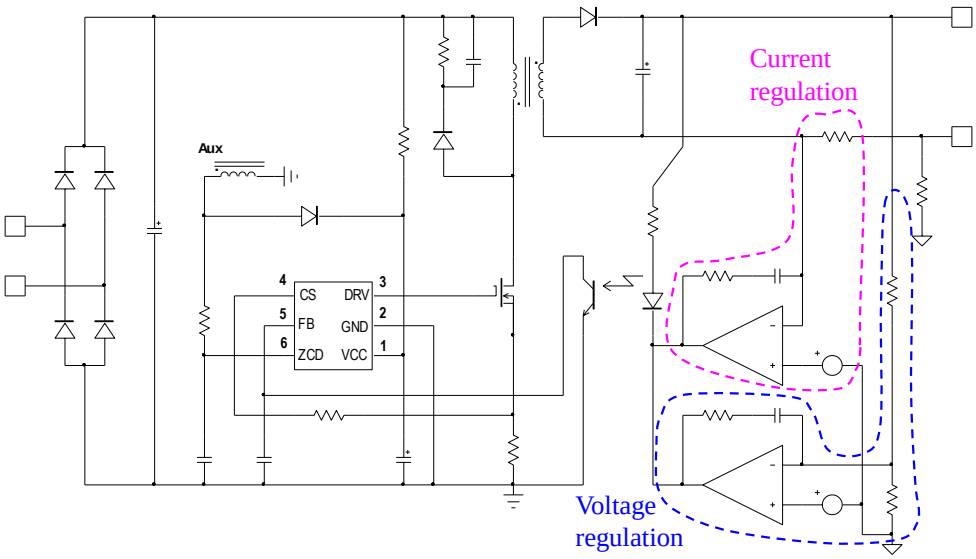


*Fig.1. Simplified flyback converter with secondary–side-constant-voltage and constant-current regulation.*

On the other hand, the PSR flyback achieves a reduced secondary-side bill of materials as pictured in Fig. 2.

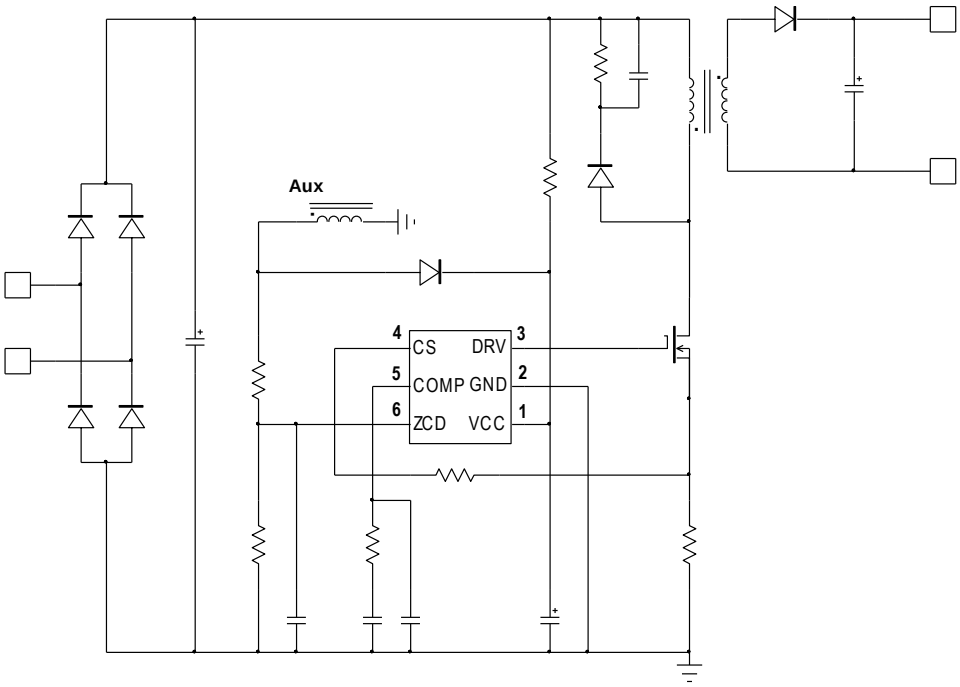


*Fig. 1. Simplified schematic of a PSR flyback.*

Primary-side CC/CV converters are generally operated in borderline conduction mode (BCM) or in discontinuous conduction mode (DCM). The output voltage is regulated by sensing the auxiliary winding voltage. Indeed, the auxiliary winding provides an image of the output voltage during the off-time of the power MOSFET. By sampling the auxiliary voltage knee (which represents the end of the core demagnetization) the controller is able to accurately control the output voltage.

The constant current regulation case differs from the constant-voltage technique in the way that there is no direct image of the output current available on the primary side. The output current is estimated by measuring the core demagnetization time and the current inside the power switch as we will see in the next section.

## *Analytical Expression For Output Current*

In order to estimate the output current accuracy, a model of the PSR constant current-current flyback is needed.

Fig. 3 shows the primary- and secondary-side currents in a flyback converter operated in BCM. When the MOSFET is turned on, the current ramps up with a slope approximately equal to the input voltage $V_{in}$ divided by the primary inductance $L_p$ until it reaches the setpoint imposed by the controller, $I_{L,pk}$. When the MOSFET turns off, the leakage inductance current subtracts from the magnetizing current and delays the output current increase. As a result, the secondary peak current is reduced:

$$I_{D,pk} < \frac{I_{L,pk}}{N_{sp}} \qquad (1)$$

where $I_{D,pk}$ is the secondary rectifier peak current and $N_{sp}$ is the turns ratio of the flyback transformer and equals the secondary winding turns number divided by the primary winding turns number ($N_{sp} = N_s/N_p$).

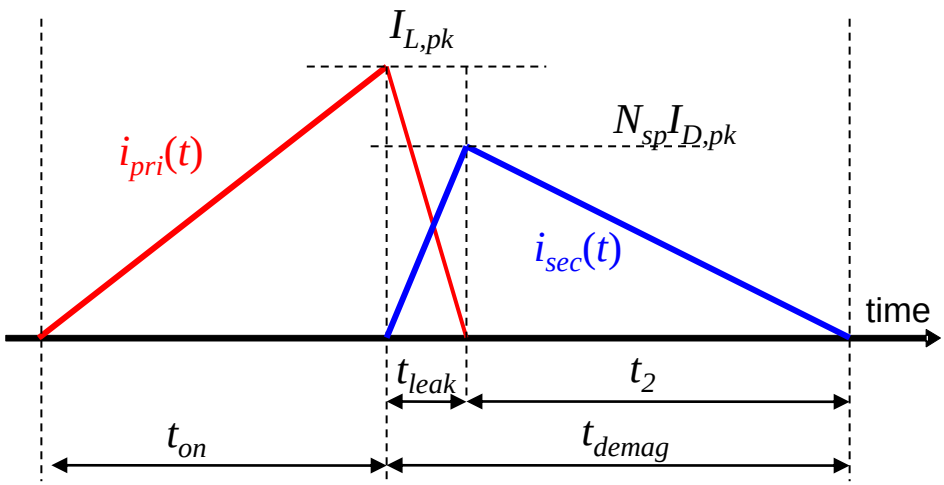


*Fig. 3. Primary and secondary current waveform in a flyback converter operated in BCM.*

The output current is the waveform $i_{sec}(t)$ averaged over one switching period $T_{sw}$ or simply the area of the blue triangle on Fig. 1. The output current expression is given by equation (1):

$$I_{out} = \langle i_{sec}(t) \rangle_{T_{sw}} = \frac{I_{L,pk}}{2N_{sp}} \frac{t_{demag} - t_{leak}}{T_{sw}} \tag{2}$$

where $t_{demag}$ is the demagnetization time of the transformer and $t_{leak}$ is the time needed to reset the leakage inductance.

Looking at this expression for the output current, we can see that the turns ratio $N_{sp}$ is a constant. Thus, in order to make the output current constant, the term $I_{L,pk} \frac{t_{demag} - t_{leak}}{T_{sw}}$ must be constant. This is what the constant current control in current-mode generally does. Most of the time, people tend to neglect the leakage inductance effect on the output current and simply monitor only the demagnetization time to control the output current:

$$I_{out} \approx \frac{I_{L,pk}}{2N_{sp}} \frac{t_{demag}}{T_{sw}} \tag{3}$$

In the end, the PSR controller implements an algorithm that controls the peak current such that:

$$I_{L,pk} = \frac{V_{CS}}{R_{sense}} = \frac{V_{REF}}{R_{sense}} \frac{T_{sw}}{t_{demag}} \tag{4}$$

Or such that

$$I_{L,pk} = \frac{V_{CS}}{R_{sense}} = \frac{V_{REF}}{R_{sense}} \frac{T_{sw}}{t_{demag} - t_{leak}} \tag{5}$$

where $V_{CS}$ is the current sense voltage seen by the controller, $R_{sense}$ is the resistor sensing the MOSFET current, $V_{REF}$ is a precise voltage reference internally provided by the controller and $T_{sw}$ is the switching period.

Replacing the peak current defined by (4) in (3), we get the final expression for the output current:

$$I_{out} = \frac{V_{REF}}{2N_{sp}R_{sense}} \tag{6}$$

Looking at (6), at first glance, it seems that the output current is independent of the magnetizing inductance. Also, since $N_{sp}$ represents the transformer turns ratio and is constant, $I_{out}$ precision only depends only on $V_{REF}$ and $R_{sense}$ precision.

In reality, because of the propagation delays ($t_{prop}$) inherent to the controller and the power switch drive, the peak current is increased by a slight amount which depends on $L_p$ and $V_{in}$. Therefore, equation (4) is updated as follows:

$$I_{L,pk} = \frac{V_{CS}}{R_{sense}} + t_{prop}\frac{V_{in}}{L_p} = \frac{V_{REF}}{R_{sense}}\frac{T_{sw}}{t_{demag} - t_{leak}} + t_{prop}\frac{V_{in}}{L_p} \tag{7}$$

In order to compensate the peak current increase brought by the propagation delays, PSR controllers feature a means to decrease the peak current setpoint as a function of the input voltage. This is usually called *line feedforward*. A simple solution consists of adding an offset to the current-sense voltage which is proportional to the line voltage. Thus, as $V_{in}$ increases, the peak current is decreased. As an example, Fig. 4 shows the line feedforward circuit that is implemented inside the NCL30082 PSR controller.

$$I_{L,pk} = \frac{V_{CS}}{R_{sense}} + t_{prop}\frac{V_{in}}{L_p} = \frac{V_{REF}}{R_{sense}}\frac{T_{sw}}{t_{demag} - t_{leak}} + t_{prop}\frac{V_{in}}{L_p} - \frac{V_{CS(offset)}}{R_{sense}} \tag{8}$$

where $V_{CS(offset)}$ is the voltage offset generated by the line feedforward circuit of the PSR controller and is defined as shown in equations (9) and (10).

$$V_{CS(offset)} = I_{RLFF}R_{LFF} \tag{9}$$

$$I_{RLFF} = K_{LFF}\frac{R_{BOL}}{R_{BOU} + R_{BOL}} - I_{CCS} \tag{10}$$

$I_{RLFF}$ is the current flowing inside $R_{LFF}$ and $I_{CCS}$ is the current charging the CS pin capacitor when the offset current $I_{offset}$ is applied to CS pin during the on-time. The line feedforward circuit will be explained in more detail later in this article.

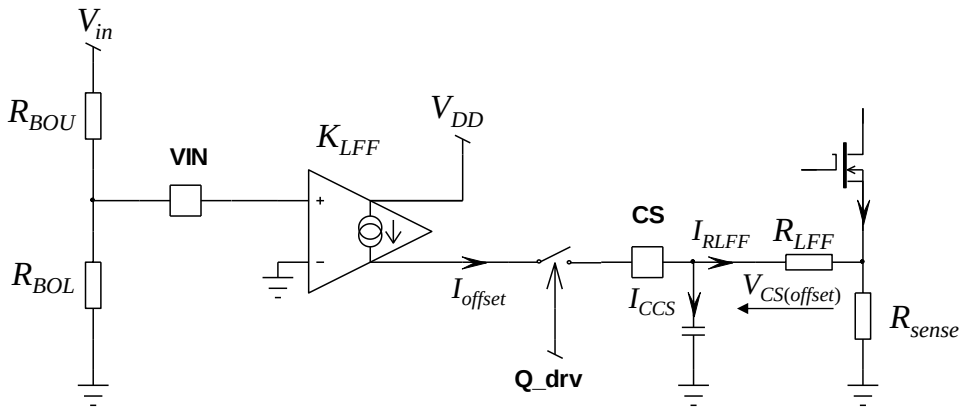


*Fig. 4. Line feedforward circuit implemented inside the NCL30082, a quasi-resonant primary-side current-mode controller.*

The peak current setpoint depends of the correct measurement of the transformer demagnetization time $t_{demag}$ by the controller. This demagnetization time is measured by detecting the knee of the auxiliary winding voltage $V_{aux}$ during the off-time (Fig. 5). The auxiliary winding is monitored by the ZCD pin of the controller (Fig. 1). An R-C network is connected on the ZCD pin to slightly delay $V_{aux}$ signal in order to turn on the MOSFET when the drain-source voltage is at its minimum value. This drain-source voltage minimum value is usually called a valley.

The R-C network delays the knee detection and thus artificially increases the demagnetization time $t_{demag}$ measured by the controller. If the time constant of this network is high, it can have a significant impact on the output current. Thus, this needs to be taken into account in the model. If we call $t_{ZCD}$ the delay introduced by the R-C network, we can update the peak current shown in equation (8) as follows:

$$I_{L,pk} = \frac{V_{REF}}{R_{sense}} \frac{T_{sw}}{t_{demag} - t_{leak} + t_{ZCD}} + t_{prop} \frac{V_{in}}{L_p} - \frac{V_{CS(offset)}}{R_{sense}} \qquad (11)$$

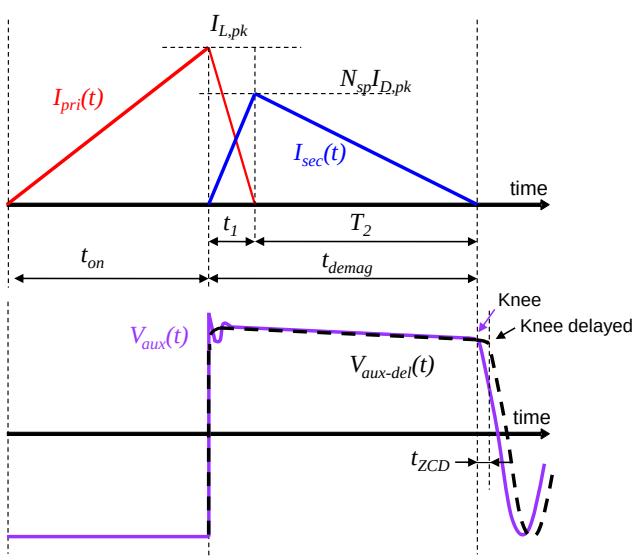


*Fig. 5. Auxiliary winding waveform.*

As a first approximation, the delay $t_{ZCD}$ can be considered equal to the time constant of the ZCD pin R-C network:

$$t_{ZCD} \approx R_{ZCD} C_{ZCD} \quad (12)$$

where $R_{ZCD}$ is the equivalent resistor seen by the ZCD pin of the controller and $C_{ZCD}$ is the value of the capacitor connected between the CZD pin and the GND pin of the controller. The value of $t_{ZCD}$ should in the range of 20 ns to 300 ns for a correctly designed PSR CC flyback .

In order to build the analytical model of the converter, we need to find an expression for the leakage inductance reset time, $t_{leak}$ in equation (11). Reference [2] gives a detailed explanation about the *RCD* clamp design according to the leakage inductance of the transformer.

Looking at Fig. 6, the *RCD* clamp limits the drain voltage increase caused by the leakage inductance $L_{leak}$ when the MOSFET turns off. The leakage inductance sees a reset voltage $V_{reset}$ equal to the clamping voltage of the *RCD* clamp ($V_{clamp}$) minus the reflected voltage of the flyback converter.

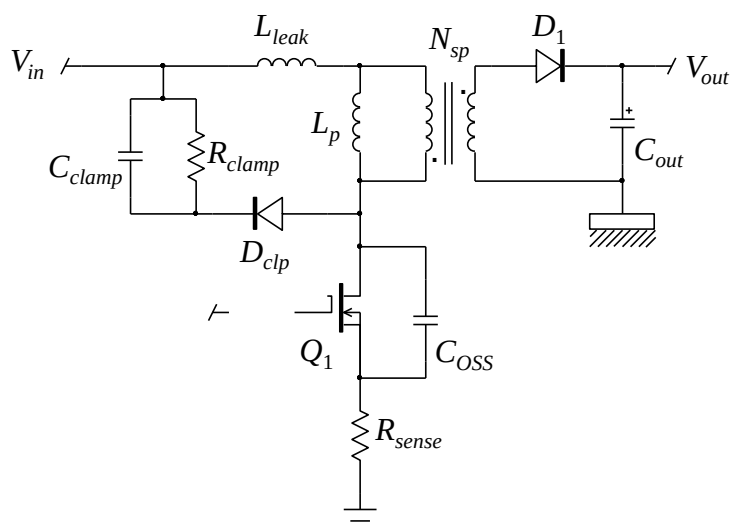


*Fig. 6. The flyback converter and its clamping network.*

Thus, the leakage inductance current ramps down with a slope $S_{Lleak}$:

$$S_{Lleak} = \frac{V_{reset}}{L_{leak}} = \left( V_{clamp} - \frac{V_{out} + V_f}{N_{sp}} \right) \frac{1}{L_{leak}} = \left( V_{clamp} - \frac{V_{out} + V_f}{N_{sp}} \right) \frac{1}{k_{leak} L_p} \quad (13)$$

In equation (13), $L_{leak}$ is expressed as a percentage of the primary inductance, represented by the $k_{leak}$ coefficient.

$$L_{leak} = k_{leak} L_p \quad (14)$$

From equations (13) and (14), we can deduce the $t_{leak}$ expression:

$$t_{leak} = \frac{I_{L,pk}}{S_{Lleak}} = \frac{N_{sp} k_{leak} L_p I_{L,pk}}{N_{sp} V_{clamp} - \left(V_{out} + V_f\right)} \tag{15}$$

According to reference [2] the mathematical expressions for $T_{sw}$ and $t_{demag}$ for a quasi-resonant converter can be approximated as follows:

$$T_{sw} = L_p I_{L,pk} \left( \frac{1}{V_{in}} + \frac{N_{sp}}{V_{out} + V_f} \right) + \left(2n_v - 1\right) t_v \tag{16}$$

$$t_{demag} = L_p I_{L,pk} \frac{N_{sp}}{V_{out} + V_f} \tag{17}$$

where $n_v$ is the operating valley number: $n_v$ = 1, 2, 3 …; and $t_v$ is the free oscillation half period:

$$t_v = \pi \sqrt{L_p \left(k_{leak} + 1\right) C_{lump}} \tag{18}$$

In equation (18), $C_{lump}$ symbolizes the total capacitance at the drain node. It includes the MOSFET drain-source capacitance and the transformer's various capacitances that are split between the windings and the primary inductance. $V_f$ is the forward voltage drop of the secondary rectifier.

Combining (15), (16) and (17) in equation (11), the peak current can finally be updated as follows:

$$I_{L,pk} = \frac{V_{REF}}{R_{sense}} \frac{L_p I_{L,pk} \left( \frac{1}{V_{in}} + \frac{N_{sp}}{V_{out} + V_f} \right) + \left(2n_v - 1\right) t_v}{N_{sp} L_p I_{L,pk} \left( \frac{1}{V_{out} + V_f} - \frac{k_{leak}}{N_{sp} V_{clamp} - \left(V_{out} + V_f\right)} \right) + t_{ZCD}} + t_{prop} \frac{V_{in}}{L_p} - \frac{V_{CS(offset)}}{R_{sense}} \tag{19}$$

Looking at equation (19), we can see that the peak current setpoint given by the converter depends on the primary inductance, the propagation delay and the clamping voltage. Thus these parameters also influence the output current, contrary to what (6) expresses.

In order to establish our analytical model for the PSR, we also need a formula for the clamping voltage. Reference [2] also conveniently provides us with the answer:

$$2V_{clamp} \left( V_{clamp} - \frac{V_{out} + V_f}{N_{sp}} \right) = R_{clamp} k_{leak} L_p I_{L,pk}{}^2 F_{sw} \tag{20}$$

Looking at (20), we can see that $V_{clamp}$ is also a function of the peak current. Also, equations (19) and (20) are both second-order equations and trying to extract by hand symbolic expressions for $I_{L,pk}$ and $V_{clamp}$ would lead to *high-entropy* results with (possible) errors. The simplest way to get a value for these parameters is to use a mathematical solver such as Mathcad and ask it to solve the system formed by the two equations. Once we have calculated $I_{L,pk}$ and $V_{clamp}$, we can also deduce the value of the output current:

$$I_{out} = \frac{1}{2} I_{L,pk} \frac{L_p I_{L,pk} \left( \frac{1}{V_{out} + V_f} - \frac{k_{leak}}{N_{sp} V_{clamp} - \left( V_{out} + V_f \right)} \right)}{L_p I_{L,pk} \left( \frac{1}{V_{in}} + \frac{N_{sp}}{V_{out} + V_f} \right) + \left( 2n_v - 1 \right) t_v} \qquad (21)$$

To summarize, the analytical model of the PSR flyback converter consists of solving the three equations (19), (20) and (21). In order to get the output current value with (21), we need first to calculate the peak current $I_{L,pk}$ with (19). Then comes the clamping voltage $V_{clamp}$ with (20) which corresponds to the operating setpoint imposed by the input voltage and the output load (the LED string set the output voltage).

In Fig. 7, we have plotted with Mathcad the output current obtained with the analytical model when the input voltage is varied from 120 V dc to 375 V dc. The output current is plotted for two different output loads:

$V_{out}$ = 20 V representing six LEDs in series

$V_{out}$ = 10 V representing three LEDs in series

The table below summarizes all the variables values used to plot Fig. 7.

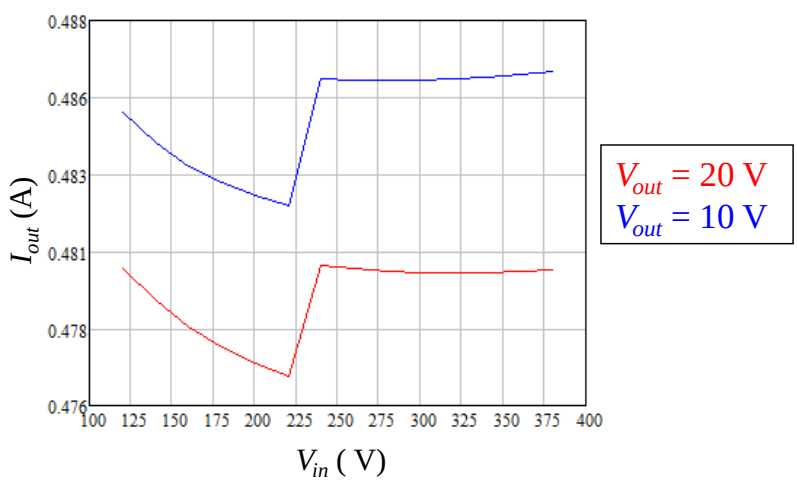


*Fig. 7. Output current variation versus input voltage.*

Table. Flyback converter design values.

| Parameter | Value |
|---|---|
| $V_{out}$ | 20 V |
| $V_{in}$ | 162 V |
| $V_f$ | 0.5 V |
| $L_p$ | 1870 µH |
| $k_{leak}$ | 0.01 |
| $N_{sp}$ | 0.17 |
| $C_{lump}$ | 60 pF |
| $n_v$ | 1 |
| $R_{clamp}$ | 270 kΩ |
| $R_{sense}$ | 3 Ω |

| | |
|---|---|
| $R_{ZCDU}$ | 24 kΩ |
| $R_{ZCDL}$ | 8.2 kΩ |
| $C_{ZCD}$ | 22 pF |
| $t_{ZCD}$ | 134.4 ns |
| $R_{BOU}$ | 9.9 MΩ |
| $R_{BOL}$ | 100 kΩ |
| $K_{LFF}$ | 17 µA/V |
| $R_{LFF}$ | 1.6 kΩ |
| $t_{prop}$ | 140 ns |
| $C_{CS}$ | 27 pF |
| $I_{CCS}$ at $V_{in}$ = 162 V dc | 6.95 µA |

In order to obtain some confidence in the accuracy of the model, measurements on a 10-W LED driver controlled by the NCL30082 were performed. Fig. 8 portrays the schematic of the 10-W LED driver. A dc voltage varying from 120 V to 375 V was applied to the board input. The output load was varied from six LEDs ($V_{out}$ = 20 V) to three LEDs ($V_{out}$ = 10 V).

Fig. 9 plots the output current variation obtained with the analytical model and the measurements obtained from the LED driver. We can see that the output current variation for this sample is quite well predicted. There is about a 1% offset between the average current predicted by the model and the measurement, but we have entered only typical values in the model. In reality, all the components on the board have an initial tolerance for their value. Also, the model does not take into account the effect of the secondary rectifier's reverse recovery time, which tends to decrease the output current setpoint.

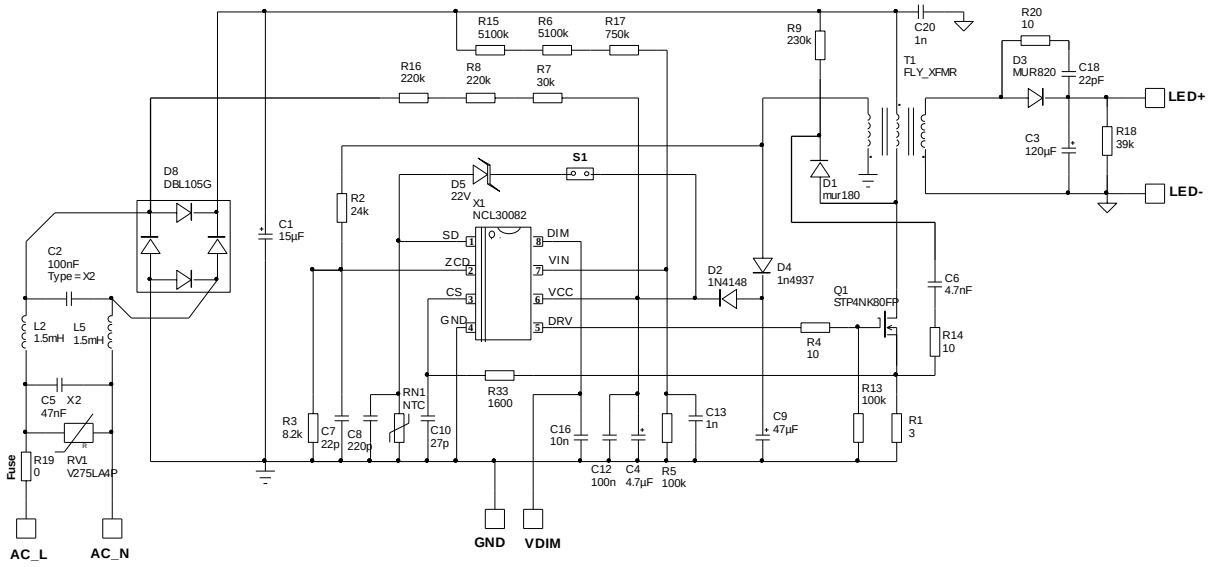


*Fig. 8. NCL30082 evaluation board schematic.*

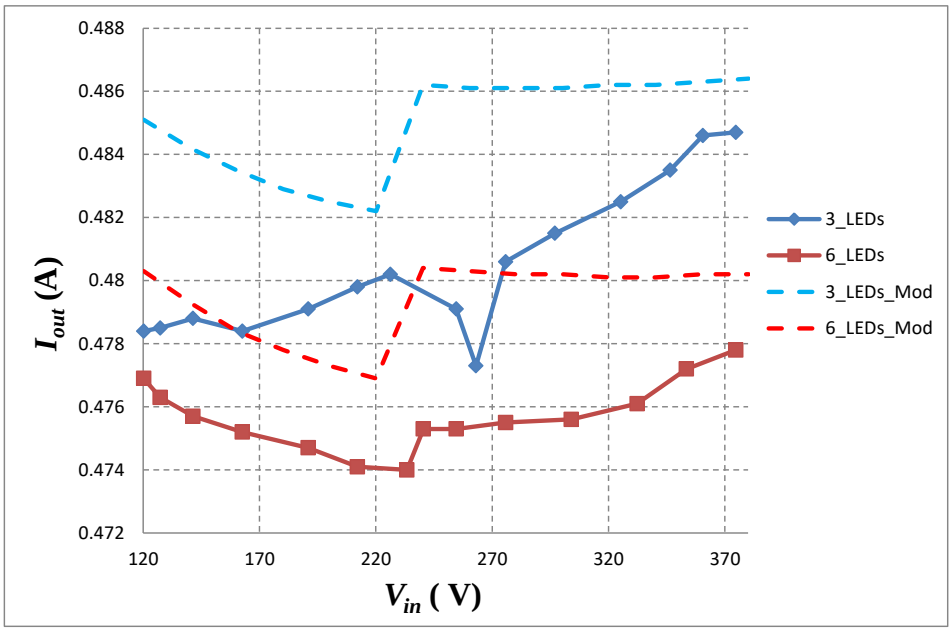


*Fig. 9. Comparison of analytical model versus experimental results.*

Here in part 1 of this article, we have derived an analytical model for the primary-side constant-current flyback and we have checked its validity by comparing the output current predicted by the model against measurements on a real PSR flyback converter. Since we now have some confidence in the model, in the upcoming parts of this article, we'll apply the full range of circuit values to obtain an estimate of the model's worst-case accuracy.

**References**

1. "Building an Average Model For Primary-Side Regulated Flyback Converters" by Yann Vaquette, How2Power Today, March 2017.

2. "Switch Mode Power Supplies" by Christophe P. Basso, , McGraw Hill, 2014.

## About The Author

*Stéphanie Cannenterre has been an application engineer at ON Semiconductor in Toulouse, France since 2006. In this role, she has developed several controllers and ASICS mainly for flyback converters. She has developed the NCL3008X controller family dedicated to LED lighting. She is currently developing controllers for single-stage PSR CC/CV converter still dedicated to LED lighting to further extend the NCL3008X family. Stéphanie graduated from the INSA (Institut National des Sciences Appliquées) engineering school in Toulouse with an MSEE degree. She holds five patents on power conversion.*

*For more information on current-mode control, see How2Power's Design Guide, locate the Design Area category and select "Control Methods".*